Heliyon 10 (2024) e39452

Contents lists available at ScienceDirect

Heliyon

journal homepage: www.cell.com/heliyon

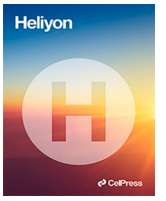

Research article

Topology optimization of coronary artery stent considering structural and hemodynamic parameters

Fatemeh Ahadi [a], Mohammad Azadi [a,*], Mojtaba Biglari [a], Mahdi Bodaghi [b]

[a] Faculty of Mechanical Engineering, Semnan University, Semnan, Iran
[b] Department of Engineering, School of Science and Technology, Nottingham Trent University, Nottingham, United Kingdom

ARTICLE INFO

Keywords:
Stent
Topology optimization
Computational fluid dynamics
Hemodynamic
3D printing

ABSTRACT

In the present study, the impact of geometric variables and structural features of stents on hemodynamic parameters is investigated. Intravascular stent implantation is a treatment method whose success largely depends on the geometric structure of the stent and its effect on hemodynamic parameters. Medical devices called stents are inserted into arteries to restore blood flow when an artery is blocked. In this research, an optimal stent was designed and its effect compared to the common commercial stent used for coronary arteries was investigated and compared. It has been found that the geometry of the stent has an effective impact on the wall shear stress in the stented artery. Therefore, in this article, the importance of stent structures in the treatment of the coronary artery disease is discussed. For this purpose, first, an optimal stent is created with the topology optimization technique to find the best structure in the stent design. Finally, the optimized stent is numerically verified with ANSYS software and compared with existing commercial stents, and then the prototype is fabricated using additive manufacturing techniques. Commercial software ABAQUS, SolidWorks, and ANSYS are used in this research. The results showed that in optimizing a square plate, a sample with a minimum residual volume limit equal to 10 and 7 % can be selected as the optimal state. The results indicate that the new design can improve the distribution of wall shear stresses to reduce the adverse hemodynamic changes. Therefore, the proposed stent geometric structure can help improve the treatment. Finally, the optimized stent along with a commercial stent was made with the 3D printing method.

1. Introduction

Accurate prediction and control of blood flow and friction within the stent-vessel interface is crucial to ensure optimal stent design and functionality. By optimizing the stent structure and considering both structural and hemodynamic parameters, researchers can minimize the friction coefficient at the stent-vessel interface. It should be noted that the effect of the friction coefficient depends on the deformation of the wall and the stent over time. This can help reduce the risk of complications such as endothelialization, neointimal hyperplasia, and restenosis. Furthermore, the optimization process takes into account various parameters such as stent strut shape and size, thickness, and overall stent diameter, which can all influence the coefficient of friction [1]. By minimizing the friction coefficient, the flow regime within the vessel can be improved, promoting better blood circulation and potentially reducing the risk of further complications [2]. By optimizing the stent design to decrease the maximum stress and increase plaque displacement, the stenosis of the

* Corresponding author.
E-mail address: m_azadi@semnan.ac.ir (M. Azadi).

https://doi.org/10.1016/j.heliyon.2024.e39452
Received 26 July 2024; Received in revised form 15 October 2024; Accepted 15 October 2024
Available online 16 October 2024

blood vessel can be decreased, ultimately improving blood flow and patient outcomes [1]. Additionally, the optimization process considers the specific conditions and requirements of different arteries. This ensures that the resulting stent design is tailored to each patient, maximizing its effectiveness and minimizing any potential negative impacts on blood flow. The coefficient of friction that the stent creates in the vessel has an effective role in changing the flow regime. By reducing the coefficient of friction, the flow regime can transition from a turbulent or transitional state to a more desirable laminar flow [3]. This transition to laminar flow is beneficial as it reduces energy loss, minimizes the risk of thrombosis and restenosis, and promotes better oxygen and nutrient delivery to the surrounding tissues [1]. In conclusion, accurate prediction and control of the coefficient of friction within the stent-vessel interface is essential for optimizing stent design and improving blood flow in the vessel. In conclusion, accurate prediction and control of the coefficient of friction within the stent-vessel interface is crucial for optimizing stent design and improving blood flow in the vessel. To summarize, the coefficient of friction created by the stent in the vessel has a significant impact on changing the flow regime. This can affect the likelihood of complications, such as endothelialization, neointimal hyperplasia, and restenosis.

Cramps can reduce and reduce blood flow. Furthermore, wall shear stress can cause occlusion, thus hemodynamic factors related to blood vessels are important for understanding physiological arterial diseases [4]. Much experimental research on flows and stents was described in 1997 [5], and many sources were used to create various mathematical models for analysis and analysis [6,7]. In addition, these studies continue in different fields for different types of stents with different uses [8].

Vascular occlusion is another major topic in this line of study [9–11]. One of the various methods for clearing artery blockage is stenting. A cylindrical scaffold called a stent is used to unblock arteries [12,13]. Stent use for coronary artery disease has significantly grown in the modern era [14]. As a result, it is crucial to analyze stent behavior mechanically [15]. The mechanical analysis of stent behavior refers to the application of solid elements and finite element theory to the study of stent behavior under various stress, temperature, and other variables. Regarding this, the mechanical analysis of stent behavior involves analyzing how the stent responds to loading and temperature by examining changes in its length, diameter, and form as well as analyzing how the intended stent changes in stress and strain [16]. Every stent topology has a unique structural and hemodynamic function, according to research on stent structure [17,18]. Furthermore, thrombosis is lessened by stent surfaces with ideal geometries [19].

Compared to other treatment methods, stenting has advantages such as no need for surgery, less pain, less complexity, and faster recovery. Therefore, the utilization of coronary stents has extended rapidly [20–22]. Moreover, stents reduce the possibility of occlusion, which is one of the most prominent reasons for the increase in stenting and the use of coronary stents. Among the most important features of stents are longitudinal flexibility, diameter reduction, expanded surface area, and their materials. Stents can be classified based on their expansion mechanism, or based on their design, or based on their materials [21,23–27].

It should be mentioned that stenting structures have an impact on arterial restenosis and thrombosis [28]. There are different types of stents, one type of stents is bioabsorbable stents which can be dissolved after providing a temporary scaffold that protects the patency of the vessel [29,30]. In addition, the results show that stent structures may have a negative effect on fluid movement in the arterial lumen and cause intima thickening [31]. It should be mentioned that following stent implantation, there is an inverse link between changes in the wall shear stresses and neointimal hyperplasia [32,33].

After implanting the stents, the wall shear stress changes according to changes in the blood flow velocity profile in the stented segment [34]. Studies have illustrated that in areas with wall shear stresses lower than 0.5 (Pa), there is a possibility of atherosclerosis due to intimal thickening, and in areas with wall shear stresses more than 2.5 (Pa), it enhances the possibility of thrombosis [35,36].

According to the mentioned literature review, it can be claimed that each stent topology has its own importance under the objectives of hemodynamic and structural issues. In this research, the topology optimization method has been used for the optimal design of stent cells. In the published papers, the topology optimization to find the suitable cell is not done. Therefore, the innovation of this research can be presented as follows:

- Finding an optimal stent with topological stability and resistance to the forces introduced by blood flow and vascular tissue and muscles, taking into account geometrical variables such as the shape of stent cells, the connection of cells to each other, the variable length and thickness of the struts, which ultimately lead to reducing the hemodynamic parameter of wall shear stress, which causes damage in the vessel
- The use of geometric constraints in connection with the 3D printing of stents and checking the 3D printing capability of the optimal stent

This article uses the topological optimization approach and related computational approaches to build a structure for coronary artery stents. The novel design enhances the stent performance, particularly in terms of its mechanical and hemodynamic characteristics, by fusing the effect of hemodynamics with topological structures. The stent design being used plays an influence on reocclusion in the vessels. According to simulation results, the improved stent exhibits lower blood flow blockage and the adverse distribution of wall shear stress linked to the stent thrombosis (ST) and the in-stent restenosis (ISR) risk factors than the commercial stents. In order to lessen the occurrence of ST complications besides the ISR brought on by mechanical structural problems during the implantation of stents and the treatment of cardiac illnesses, the new stent structure can thus profit from a decrease in the frequency of mechanical fractures and failures, besides the adverse hemodynamic effect.

Notably, this work is not concerned with tailored, patient-specific designs, but rather with the overall design of a new kind of stent structure. In contrast to biomaterial, patient, clinical, and operational factors, this work highlights the significance of mechanical and hemodynamic structural failures.

2. Research method

2.1. Lame's law

In this part, the first goal is to obtain the optimal stent, so the structure is examined, and in the topology optimization discussion, only the solid structure is discussed. After obtaining an acceptable geometry in terms of the geometry and the topological stability, in the next part to confirm and compare the hemodynamic parameter of the optimal stent with the commercial stent, the wall shear stress parameter, which is caused by the blood flow passing over those struts, has been investigated which is the fluid analysis.

The objective of the present research is to design coronary artery stents with an optimization method. Various forces are applied to the stent.

The Lame's law for a thick cylinder relates the stress and strain in a cylindrical object, such as a stent, considering the thickness effect of vessel walls. In the context of stent-vessel interaction, the Lame's law can be used to understand the formulation between the tensile stress applied by the stent on the vessel wall and the strain or deformation caused by the vessel.

As shown in Fig. 1, a cylinder with a specific length (l), inner radius (a), and outer radius (b) is considered, which is subjected to uniform internal and external pressure P_a and P_b, respectively.

Three mechanical stresses applied to a cylindrical object are Hoop Stress, Radial Stress, and Longitudinal Stress. These stresses, shown in Fig. 1, are introduced in Table 1.

2.2. Materials

The studied material in the present research is polylactic acid (PLA). This polymer is a common material that utilized through the prototyping techniques in the manufacture of polymeric stents, as well as biomechanical and biological items that are created using 3D printing technology. Then, Table 2 depicts the mechanical characteristics of PLA in this study.

2.3. Forces in stent design

The creation of a coronary artery stent using an optimization technique is the primary objective of this study. Several stresses are exerted on the stent within the container. To optimize stent topology, it is challenging and necessary to understand the complex environment of intravascular flow and the interaction between stents, endothelial cells, and the blood flow in practice. Therefore, it is essential to exactly consider the various forces that are applied to the stent inside the vessel. In this research, all the forces, including the force from the vein and muscle tissue, as well as the force from the blood flow, are considered. These forces and dimensions of the desired coronary artery stent are shown in Fig. 2. The majority of research employs a single number for the maximum compressive force that the vessel can exert, which is between 200 and 275 mmHg, according to the results that were taken from the analysis of the papers [39]. They calculate the pressure differential between the outside and interior of the artery to be 175 mm Hg, assuming an average pressure inside the typical duct of about 100 mm Hg [39]. Additionally, the research shows that 300 mm Hg is the lowest permissible collapse pressure for coronary stents [39]. Therefore, according to the review of articles, in this research, assuming the average pressure inside the normal duct is about 100 mm Hg, the difference between the pressure outside and inside the artery is 175 mm Hg.

To optimize the calculations and since the stents are made of repeating cells, according to the problems related to the physics of the

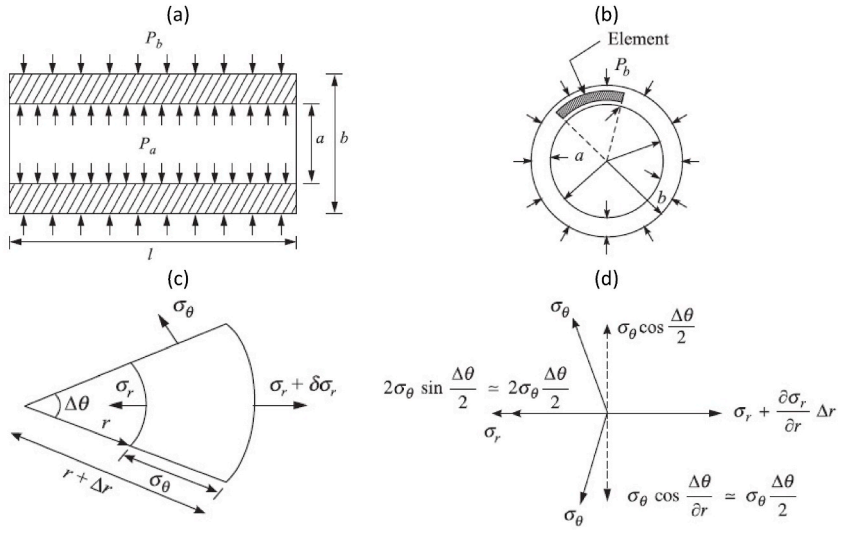

Fig. 1. The Lame's law for a thick cylinder.

Table 1
The mechanical stresses applied to a thick cylinder.

General equations	
Hoop stress	$\sigma_\theta = A + \frac{B}{r^2}$
Radial stress	$\sigma_r = A - \frac{B}{r^2}$
Boundary conditions for a thick-walled cylinder	At $r = a$, $\sigma_r = -P_a$ At $r = b$, $\sigma_r = -P_b$
Constants	$A = \frac{P_a a^2 - P_b b^2}{b^2 - a^2}$ $B = \frac{a^2 b^2 (P_a - P_b)}{b^2 - a^2}$
Lame's equations	
Hoop stress	$\sigma_\theta = \frac{P_a a^2 - P_b b^2}{b^2 - a^2} + \frac{a^2 b^2}{r^2}\left(\frac{P_a - P_b}{b^2 - a^2}\right)$
Radial stress	$\sigma_r = \frac{P_a a^2 - P_b b^2}{b^2 - a^2} - \frac{a^2 b^2}{r^2}\left(\frac{P_a - P_b}{b^2 - a^2}\right)$
Longitudinal stress	$\sigma_L = \frac{P_a a^2 - P_b b^2}{b^2 - a^2}$

Table 2
The mechanical characteristics of PLA [37,38].

Mechanical characteristics	Value
Density (g/cm^3)	1.24
Poisson ratio (−)	0.36
Elastic modulus (MPa)	3500
Yield stress (MPa)	70

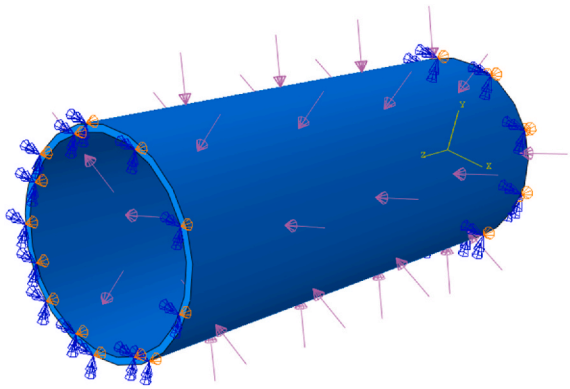

Fig. 2. The diagram of the forces acting on the intravascular stent and the blood flow.

problem according to Fig. 2, a part of the cylinder was selected for analysis.

2.4. Design domain

Blood flows through the intimal lumen in the stented section of the artery, filling in the spaces between the stent legs. To represent a stent cell, the 3D domain for computations domain based on the microstructure of stenting is developed; Fig. 3 illustrates its dimensions. In the computational domain for the stent geometry, a constant thickness is considered. Blood flows across the stent site and therefore the pressure and force exerted by it are taken into account in the calculations.

The scope of the design is shown in Fig. 3. A grid is utilized to discretize the design domain because of its accuracy and computational efficiency. Coronary stents consist primarily of closed-cell units and have a cylindrical shape.

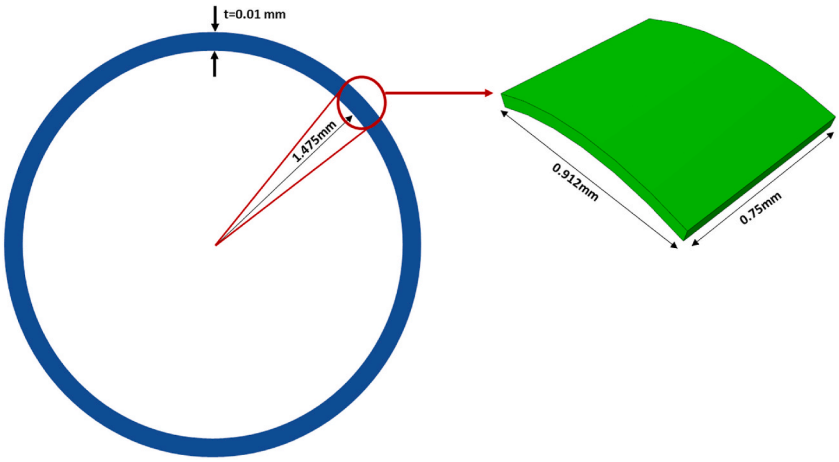

Fig. 3. The dimensions of the primary stent cylinder along with its solution strategy.

3. Results and discussion

3.1. Optimization procedures

The goal in this research is to use optimization techniques to construct a coronary artery stent. In these procedures, one cell was optimized first, and the necessary stent structure was created by repeating and assembling this cell. Based on sensitivity and finite element analyses, topology optimization was carried out. The elements' properties were established at every step. Additionally, mathematical programming methods were applied to achieve response convergence. In analyzing this problem, the goal is to reduce the wall shear stresses caused by the stent. Therefore, it is considered as the objective function to minimize the strain energy and then to minimize the volume. Moreover, the constraints of minimum stress and maximum stress are applied to the problem. Therefore, to achieve a stable and optimal stent structure, by minimizing the strain energy as the objective function, and defining the volume fraction and stress as the constraints of the problem [40–42], the optimal stent structure was obtained, which ultimately led to a decrease in the hemodynamic parameter of the wall shear stress [33]. Strain energy criteria is a universal benchmark method for multi-objective optimization, which is also considered in this study [40]. Therefore, participation in the investigation of these techniques is done in the structure optimization method using linear static analysis through the finite element modeling [40]. Then, after obtaining the optimal stent, the amount of displacement due to the application of blood flow pressure (10665.8 Pa, diastolic blood pressure) is calculated, and in the second step, taking into account the constraint of displacement to open the stent to the appropriate diameter, finally the main structure is obtained. The topology optimization solution algorithm in ABAQUS software is depicted in Fig. 4.

3.2. Mesh convergence

Mesh convergence is important in topology optimization to obtain the shape of the stent cell and accurately capture its effects. The selected surface is regularly gridded. Various mesh sizes were explored to discretize the problem to make the mesh independent and determine the least number of mesh elements with which reliable computations may be conducted. The initial mesh was the coarsest, and mesh 14 and mesh 15 produced results that were reasonably near to one another. Thus, mesh series 14 was selected to carry out the remainder of the solution. Fig. 5 displays the mesh convergence diagram together with the applied stress as a function of element count. The mesh selected as a result of mesh convergence contains 112,500 elements as shown in Fig. 6.

3.3. Optimization results

In the topology optimization technique, the main goal is to obtain the optimal structure with an appropriate distribution of the material inside the stent structure. To evaluate the overall impact on the optimal design by removing inefficient materials from the structure, areas where the amount of the strain energy is relatively low, a target design is considered, where the geometry is balanced and optimized by these factors [40]. For material structural topology optimization problems, as seen in the articles in the field of topology optimization, such as references [8,41,42], there is a volume and mass limitation, and designs are presented from the interpolation of the results. Most stents have a small volume fraction of material. Examples of the optimization of stents with different methods can be seen in Refs. [43,44], which according to the alternative model and flow pattern conditions in each of the studies, have come to the conclusion that stent bases are the most effective for improving intravascular hemodynamics. Variations in volume fraction during optimization can produce disparate outcomes. The amount of 50 % is used as the volume fraction in this study. Then, the next plans with a lower volume fraction are determined by evaluating the plan with a volume fraction of 50 %. Fig. 7 displays the

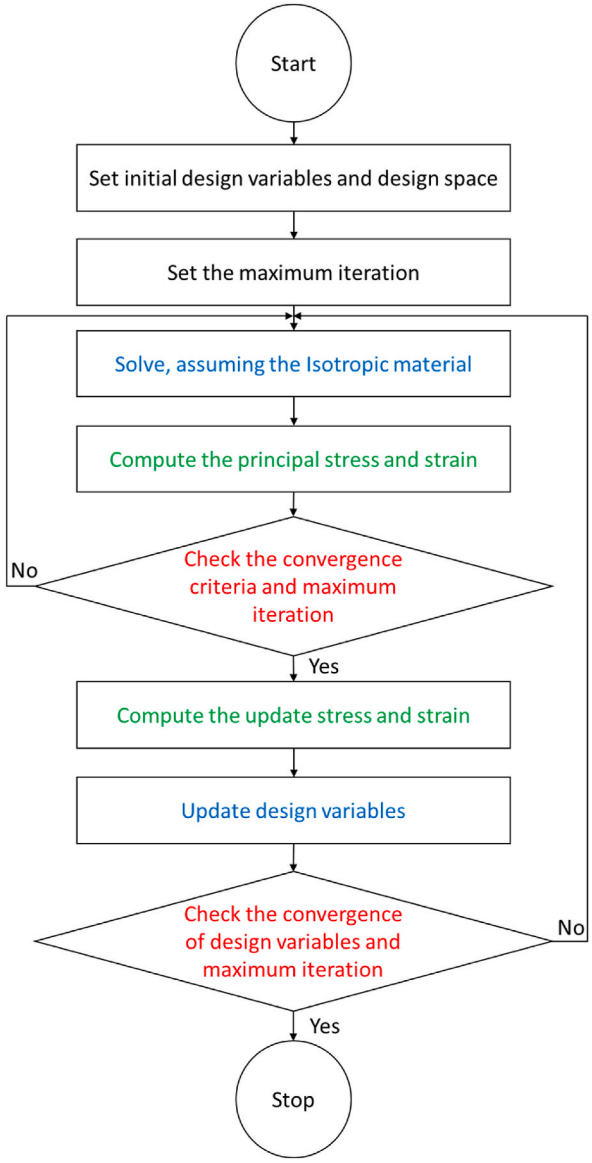

Fig. 4. The solution algorithm for the topology optimization.

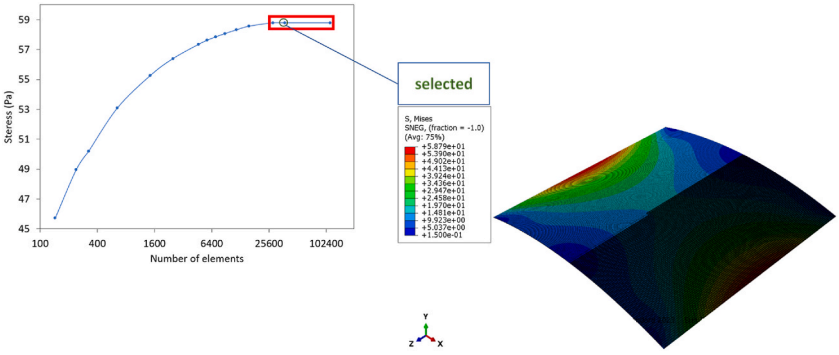

Fig. 5. The mesh convergence diagram.

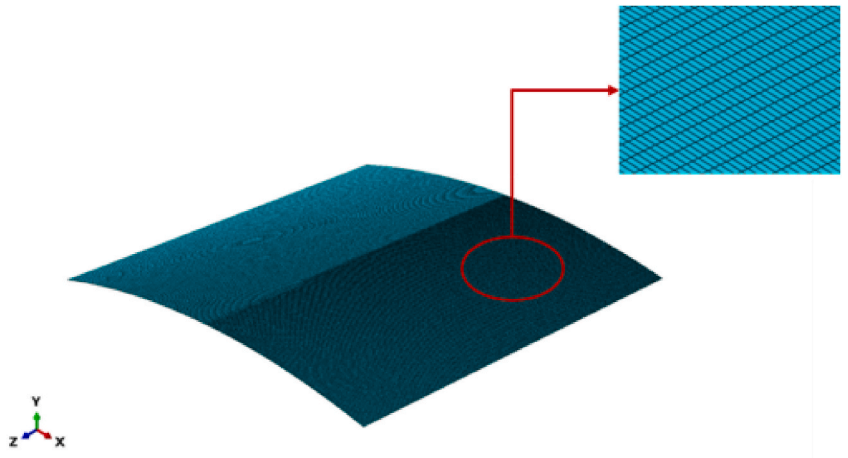

Fig. 6. The selected mesh for a stent cell.

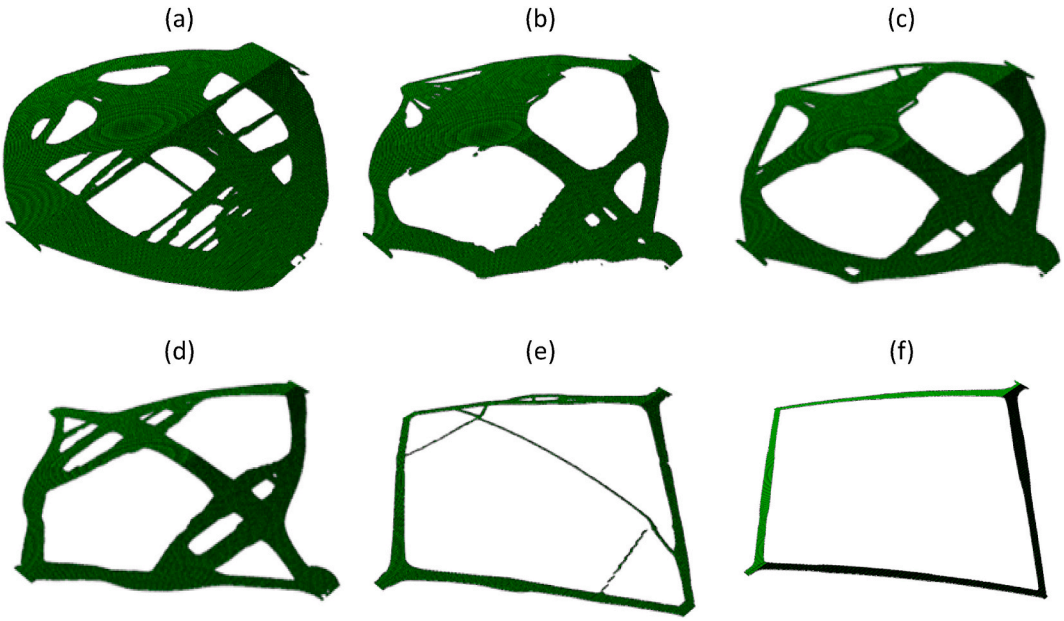

Fig. 7. The result of optimization for a square curved plane in (a) 50 %, (b) 40 %, (c) 30 %, (d) 20 %, (e) 10 %, and (f) 7 % of the volume constraint.

optimization results, considering the volume fractions ranging from 50 % to 7 %. Four intermediate data are utilized to monitor the dynamic alteration of the structure boundary throughout the optimization procedure, as depicted in Fig. 7(b)–7(e). Fig. 7(a) and (f) depict the original concept and the ultimate outcome, respectively, highlighting the differences between the two. The optimal structure for the material distribution is not uniform, as can be observed. Geometric variables including the shape of the stent cells and the placement of the stent struts, the link connecting the cells to each other, the angles between the struts, and the variable length and thickness of the struts in the longitudinal direction are important in the optimal stent. In addition, the results of iteration in stent cell optimization are presented in Fig. 8. To be sure, the convergence graph of the objective (minimization of the strain energy) in terms of iteration is also drawn in Fig. 9. As this figure shows, the topology optimization can be used as a design method to reduce the material without affecting the performance of an object, the goal being to achieve a reduction in the material usage while minimizing the strain energy. Finally, the final shape of the stent is depicted in Fig. 10.

Table 3 shows a comparison of the volume and mass changes of the initial state of the cylinder before topology optimization and the commercial stent and optimal stent. As it can be observed in Fig. 11, the stress and strain results in the cylinder (input geometry for topology optimization), the optimized stent, and the commercial stent under the applied loads are shown. The optimal stent is designed as a result of the goal of reducing the shear stresses of the wall caused by the stent, in line with which the minimization of the strain energy and the minimization of the volume is used as the objective function. As it is known, the stress and strain in the optimal stent are

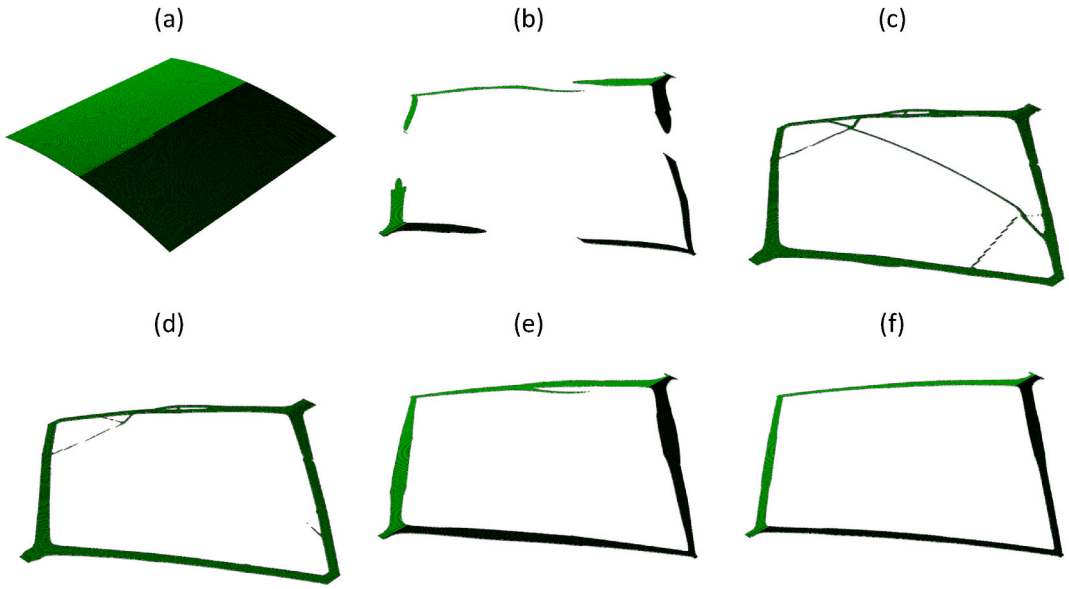

Fig. 8. The results of iteration for a square curved plane at the iteration of (a) 0, (b) 5, (c) 10, (d) 20, (e) 30, and (f) 50.

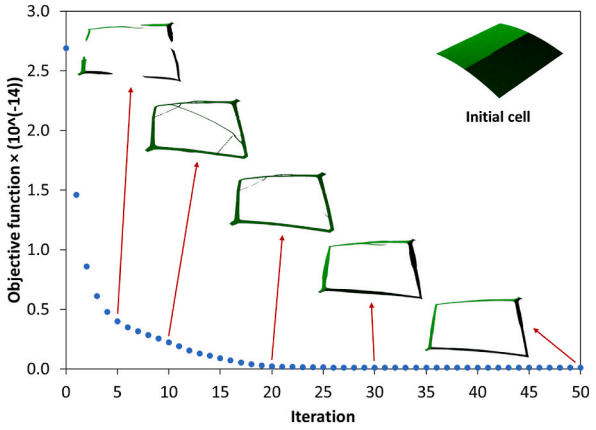

Fig. 9. The convergence diagram of the objective (minimization of the strain energy) according to the iteration.

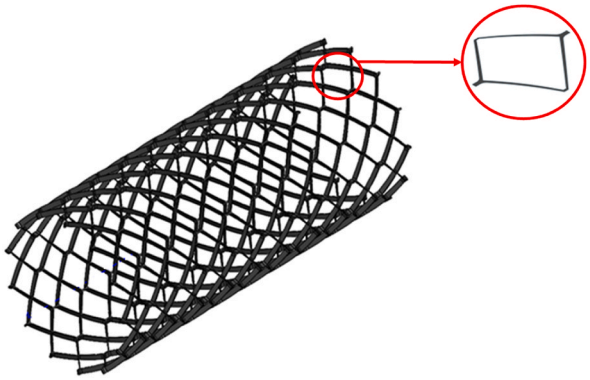

Fig. 10. The geometry of the optimized stents.

Table 3
The comparison of the volume and the mass in all case studies.

Structure	Volume (m^3)	Mass (kg)
Cylinder	7.30×10^{-9}	9.06×10^{-6}
Optimal stent	4.88×10^{-10}	6.05×10^{-7}
Commercial stent	1.75×10^{-9}	2.17×10^{-6}

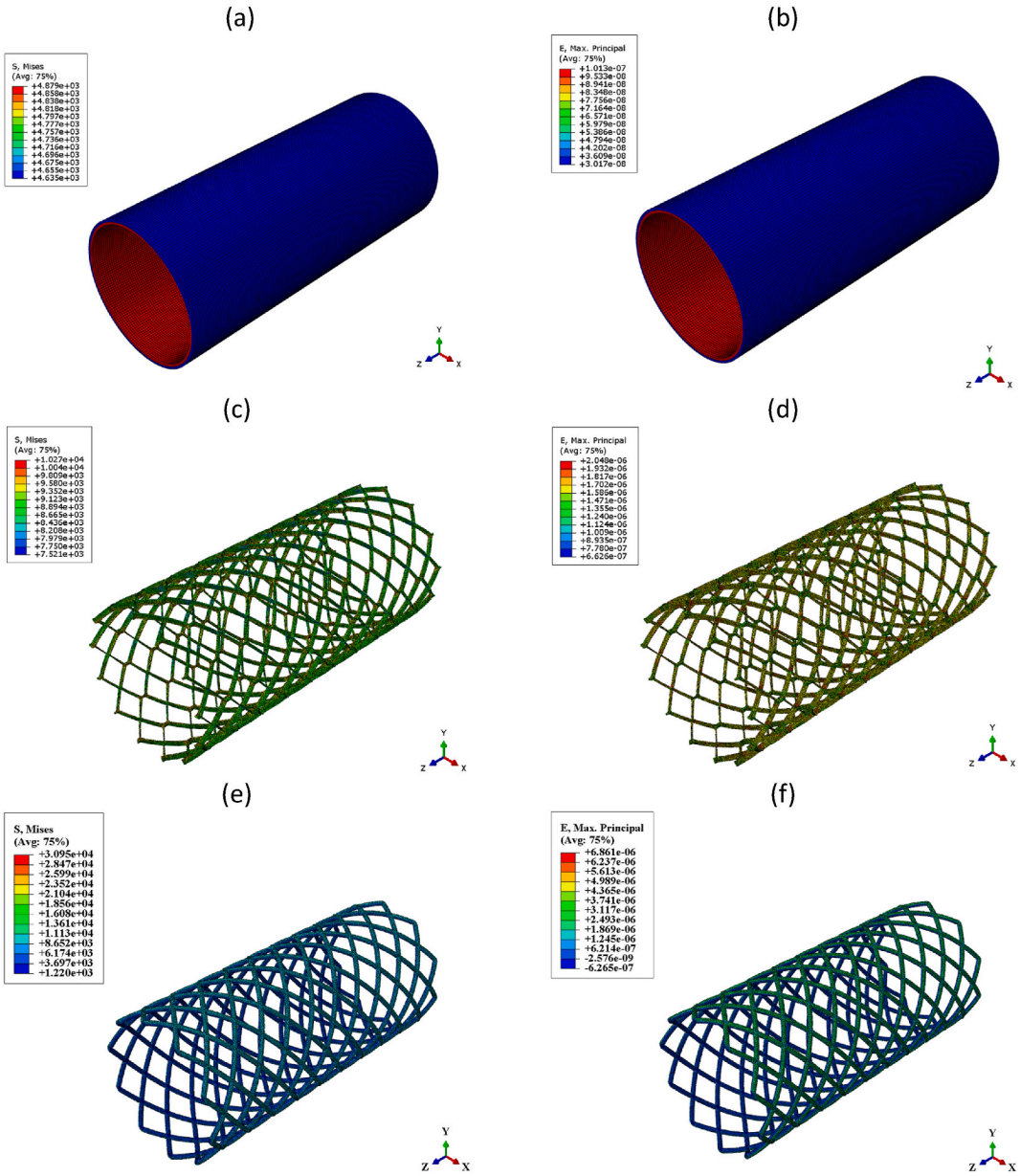

Fig. 11. The contours for (a) the stress in the cylinder, (b) the strain in the cylinder, (c) the stress in the optimal stent, (d) the strain in the optimal stent, (e) the stress in the commercial stent, and (f) the strain in the commercial stent.

less (according to the objective functions in the topology optimization process) and the highest stress and strain in the stent occurs at the junction points of the cells and in the crown of a cell, which effectively the stresses and strains in the stent are transferred from the side of the crown of the cell to the arm of the struts. In addition, since stent struts are mainly loaded in bending in flow, varying the thickness of the struts along the length of a strut in an optimized geometry causes less stress and strains on the crown.

3.4. Comparison of wall shear stress

This subpart belongs to the validation of numerical data for the performance of the optimized stents, comparing to the commercial stents. In this study, the goal was to optimize the topology of the stent, and based on this objective, the topological stability was obtained in the design of its structure. Moreover, in order to investigate and validate the improvement of the effect of the optimal stent compared to the commercial stent in improving and reducing the effective hemodynamic parameter in the blood flow through the stent, numerical modeling and simulation was also done, the solution algorithm and its results are given below.

In Fig. 12, the outline of two commercial and optimized stents along with their cell shape is given for comparison. Reduction of stent-induced adverse hemodynamics can be achieved by reducing stent obstruction to blood flow. In studies, wall shear stress is used as an accepted criterion for measuring stented hemodynamics. Therefore, the commercial stent geometry is simulated with the optimized stent in ANSYS software to validate the macroscopic performances.

In this research, the FLUENT software is utilized to simulate the flow. For this objective, the FLUENT software requires several data for the implementation of the solution in order to fix this issue. The model or the solution technique, the material qualities besides the boundary conditions for a particular problem, and the beginning conditions needed for the method of solving the problem, which are subsequently specified as all parameters, are among the necessary data. SIMPLEC algorithm and pressure-based solver were used to solve the equations in this study with specified boundary conditions. The velocity (for the boundary conditions) was set to 0.105 m/s at the inlet part [45] and then, the outlet pressure was considered at the outlet section, and finally, for the blood flow walls, the wall condition was also evaluated. In addition, the input parameters for the considered Newtonian flow include density and viscosity, which are considered to 1060 (kg/m^3) and 0.0035 (kg/ms), respectively [46–48]. The steady-state flow was also evaluated as laminar and incompressible. Moreover, the gravity acceleration was considered equal to 9.81 (m/s). In the process of finding the solution, the residuals all reached the value of 10^{-6} and converged. In addition, the mesh convergence diagram for flow with stent effect is shown in Fig. 13.

The coefficient of friction between the vessel wall and the stent structure has an effective role in determining the flow regime inside the vessel. This friction coefficient affects the shear stresses on the surface of the vessel wall and can have an effective influence on the stability and formation of thrombus inside the vessel. The computational fluid dynamics solution algorithm in the ANSYS software is depicted in Fig. 14. As it can be observed from the data in Table 4, the wall shear stress is significantly reduced in the optimized stent. This decrease in the minimum, maximum, and average wall shear stress is equal to 27 %, 17 %, and 16 %, respectively. In addition, the diagram for wall shear stresses is shown in Fig. 15, for both stents. Based on these data, the amount of wall shear stresses decreases when using the optimal stent, also using the optimal stent compared to the commercial stent, the average shear stress decreases by 16 %, which is a significant number.

According to the results of this research and by signing with reference [49], it can be shown that low-velocity areas in the vicinity of the stent cause areas with low wall shear stress, due to the decrease of the velocity gradients in the wall. Wall shear stress is maximal at the area that the flow meets the inner surface of the striae (the furthest surface from the artery wall) and is effectively decreases in the areas between the strata. The results indicate that areas of low wall shear stress between stent struts were more prominent at peak flow velocity downstream of a strut compared to that one at upstream of the following base.

In addition, research suggests that acute distribution of wall shear stress occurring immediately after implanting may predispose vessels to potentially harmful distribution of wall shear stress. Therefore, the present data suggests that the acute wall shear stress distribution observing in the stent simulation may have an effective role in creating the deleterious wall shear stress distribution that is associated with the restenosis after the implantation. Such a hypothesis is also considered in the literature, by Wentzel et al. [32] who observed the clinical evidence of restenosis in such areas. Considering all these results furtherly suggests that the environment of the blood flow created by the stent immediately after implanting may influence the distributions of wall shear stress [50].

3.5. Comparison of 3D-Printed stents

The introduction of 3D printing technology has revolutionized many industries, including healthcare. One particular area of interest is the fabrication of stents using 3D printing. Therefore, in the following, both samples of commercial stents and optimized stents with scale are printed. The reason for addressing this discussion, in addition to the examined parameters, is the comparison and the capability of 3D printing of the optimal stent next to the commercial stent. Stents are made with UltiMaker 3D printer and DURAMIC 3D PLA filament. 3D printing variables are reported in Table 5. The images of the 3D-printed stents are depicted in Fig. 16. To compare the printing quality of stents, the models printed in this article can be compared with reference [51].

In the field of medical equipment manufacturing, 3D printing and additive manufacturing has gained high attention due to its capability to fabricate complex and customized structures with high precision. This process involves building 3D objects layer by layer from digital designs. In this field of vascular stents, 3D printing allows the creation of stents with features tailored to individual needs.

Therefore, in this research, the potential of 3D printing technology in developing biodegradable vascular stents with suitable features to improve clinical outcomes is demonstrated, and this section provides insights into the design considerations and manufacturing processes involved in creating advanced medical devices with demonstrations of the utilization of additive manufacturing.

4. Validation of numerical results

After 3D printing of the stents, the hemodynamic behavior of the fluid in the vessel, with the topology-optimized stent was

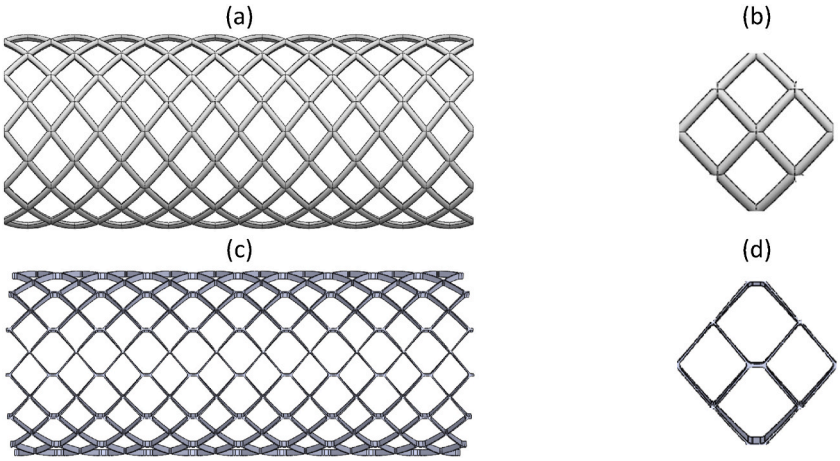

Fig. 12. The schematic images for (a) the commercial stents, (b) the commercial stent cells, (c) the optimal stents, and (d) the optimal stent cells.

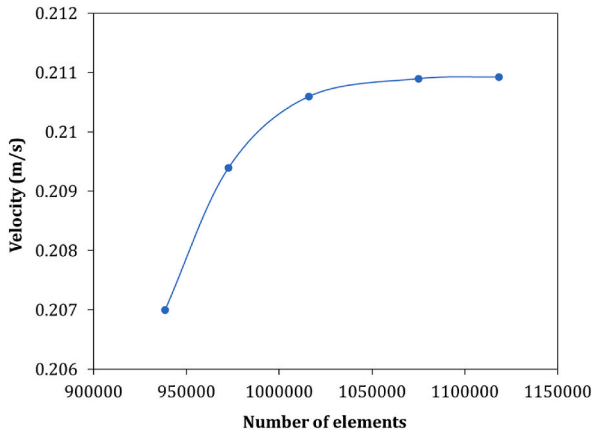

Fig. 13. The mesh convergence diagram for the flow with the stent effect.

experimentally investigated. In this section, the velocity profile is obtained within the in-vitro mock experiment and by the Particle Imaging Velocity (PIV) technique in an artificial vessel. In this test-rig, after the flow passes through the stent, the results were compared with the numerical solution by the Computational Fluid Dynamics (CFD). To ensure the numerical solution, this test was performed in a blood circulation simulator tester. As seen in Fig. 17, an imaging setup was used to apply the PIV technique to image the flow after stenting in the vessel.

A single camera (Imager Pro-X, LaVision GmbH) with a 105 mm f/2.8 lens (Micro-Nikkor) was used to capture the images, which were aligned and calibrated before using. A 532 nm pulse laser was used to illuminate the channel from the front to visualize the movement of particles in a configuration. A progressive cavity pump (Type MD 012-12, Seepex Inc.) was also utilized to maintain a steady flow. This setup used the glass bead tracer particles with a diameter of 10 μm (TS10, Dynoseeds) for imaging. Finally, the commercial software (DaVis 8.4, LaVision GmbH) was used to calculate the velocity vectors from the images obtained from the experiment.

The results in Fig. 18 show that the laboratory test correctly evaluated the performance of different profiles, and the in-vitro testing data analyzed with the PIV technique and the CFD results were in a good agreement with each other. Notably, in Fig. 18, u^* is the normalized velocity (velocity/maximum velocity), y is the location along the diameter, and finally, D is the vessel diameter. The error percentage between the numerical results and the experimental data was about 1 %. Therefore, as seen, according to the test results and the simulation data, it can be claimed that the results were completely consistent.

5. Conclusions

The effect of topology optimization and modeling of the new stent designer shows a large improvement in mechanical performance compared to the old design, suggesting that modern-designed stents have lower values for maximum stress. These are related to the core function of topology optimization to remove model material in these critical situations automatically. This paper presented a new

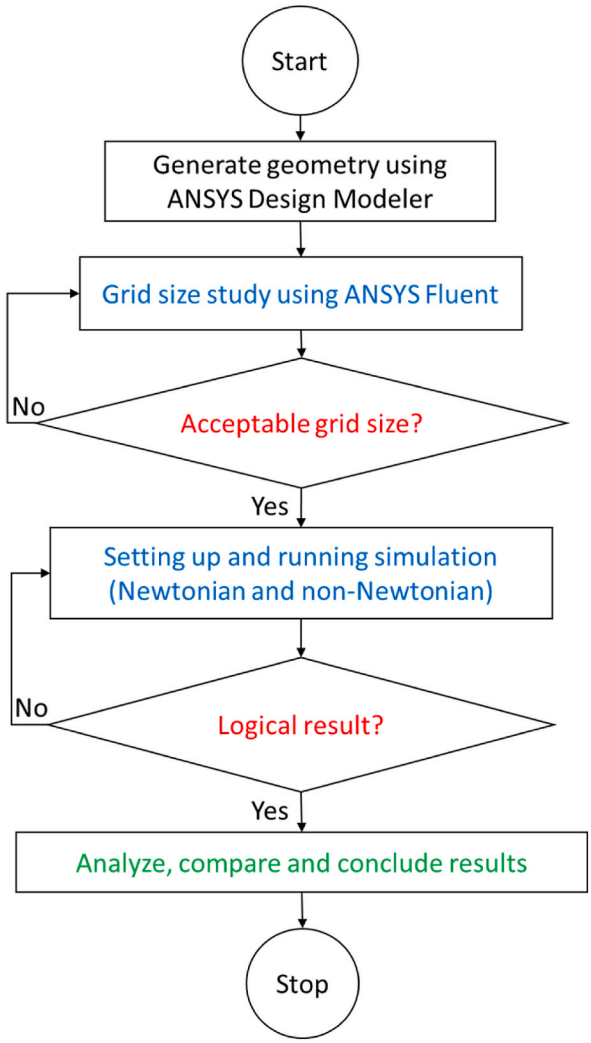

Fig. 14. The solution algorithm for computational fluid dynamics.

Table 4
The comparison of the wall shear stress in commercial and optimal stents.

Stent	Minimum wall shear stress (Pa)	Maximum wall shear stress (Pa)	Average wall shear stress (Pa)
Commercial	0.00063	7.78052	0.74079
Optimal	0.00046	6.47371	0.62257
Difference (%)	27 %	17 %	16 %

approach to stent modeling based on topology optimization. Moreover, the important factor in stent hemodynamics discussion, which is the wall shear stresses in the stent, is simulated and investigated for the optimized stent with commercially available stents, and as seen, this value is reduced in the optimized stent.

In general, the contents and results presented in this research can be expressed as follows:

- The material used in this research is PLA, which shows good performance in terms of mechanical and clinical behavior.
- The proposed method for optimization offers the advantage of avoiding human errors during the design process. It also helps reduce expensive optimization efforts during mechanical testing.
- An important and influential factor in this matter is the shear stresses of the wall.
- The optimized stent shows a reduction in wall shear stresses compared to existing stents in the market. Specifically, the average shear stress is reduced by 16 % with the optimal stent.
- Both the optimized stent and the commercial stent were produced using 3D printing.

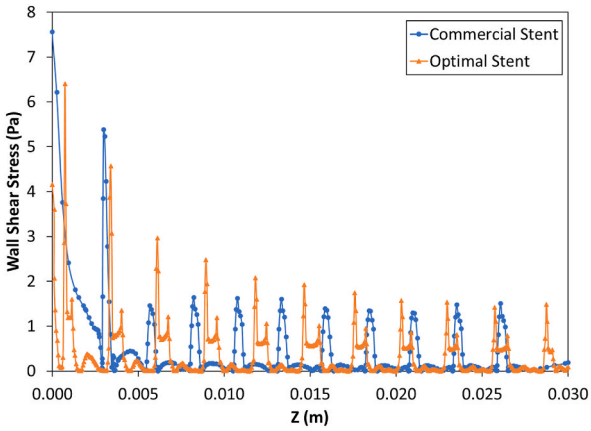

Fig. 15. The diagram of the wall shear stress on struts in the commercial stent and the optimal stent.

Table 5
The used 3D printing parameters in this research.

Parameter	Value
Layer thickness (μm)	50
Infill percentage (%)	100
Printing speed (mm/s)	5
Nozzle temperature (°C)	180

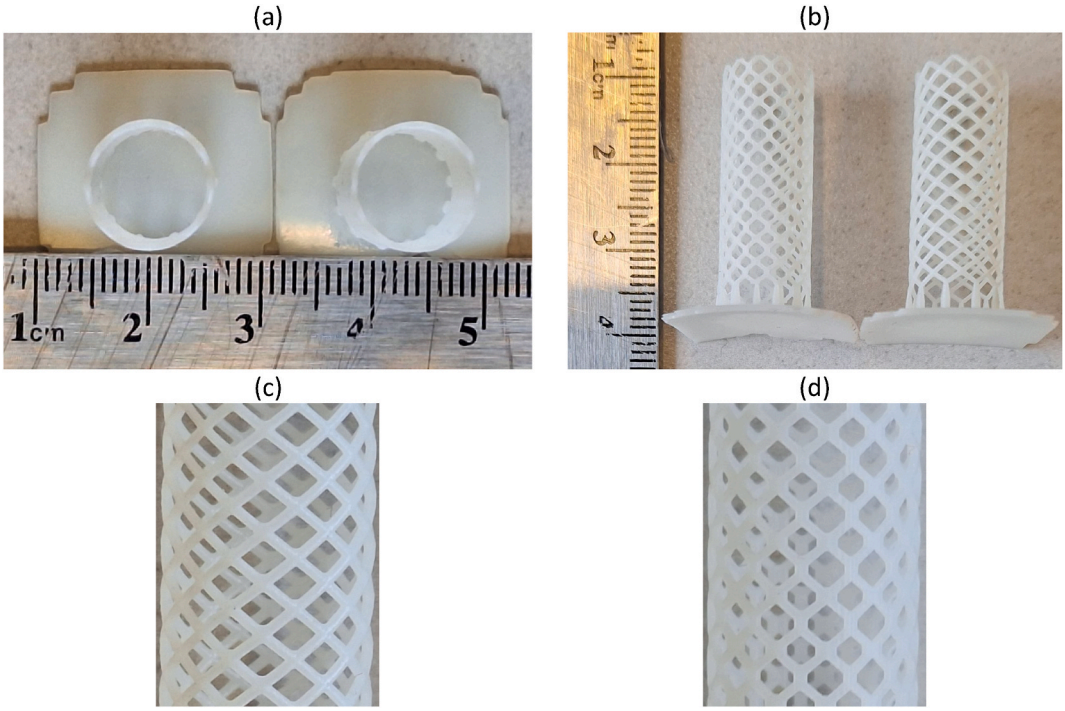

Fig. 16. The 3D-printed stents with (a) top and (b) side views plus (c) the commercial stent and (d) the optimized stent.

- The results including the velocity profile were shown by the in-vitro experiment and the particle imaging velocity technique in an artificial vessel, which had a proper agreement with the data of the computational fluid dynamics numerical solution. The relative error percentage between the numerical and experimental results was about 1 %.

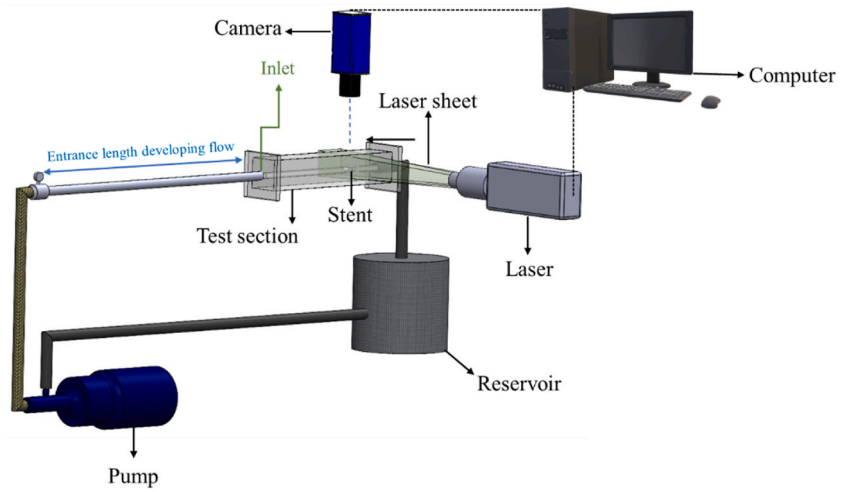

Fig. 17. The schematic image of the experimental imaging setup withing the in-vitro mock, stented artery device.

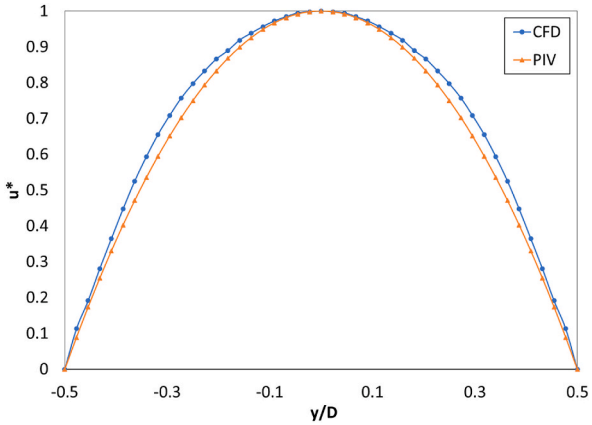

Fig. 18. Comparing the velocity profile results with PIV and CFD.

CRediT authorship contribution statement

Fatemeh Ahadi: Writing – original draft, Visualization, Software, Resources, Investigation, Formal analysis, Data curation. **Mohammad Azadi:** Writing – review & editing, Visualization, Validation, Supervision, Resources, Project administration, Methodology, Investigation, Funding acquisition, Conceptualization. **Mojtaba Biglari:** Supervision, Resources, Project administration, Methodology, Investigation, Conceptualization. **Mahdi Bodaghi:** Visualization, Supervision, Resources, Project administration, Conceptualization.

Data availability

The data that support the findings of this article are available based on the request from the corresponding author.

Funding

The research for this paper was funded by the INSF (Iran National Science Foundation), with the project number of 4004237.

Declaration of competing interest

The authors declare that they have no known competing financial interests or personal relationships that could have appeared to influence the work reported in this paper.

There is no conflict of interest for this research on behalf of all authors.

Then also for USA sanctions, we have declared that

1) All three-first authors are from academic (research and education) institutes. Moreover, authors have confirmed 2(b)(i) and 2(b)(ii) parts on the OFAC compliance.

Therefore, none of authors, how are submitting this manuscript, are as an official representative or on behalf of the government.

References

[1] X.M. Wang, P. Liu, H. Liang, M.C. Zhang, L. Li, Z.F. Yue, Analysis of the whole implementation process and optimization of a Nitinol superelastic stent, Mater. Werkst. 50 (1) (Jan. 2019) 44–51, https://doi.org/10.1002/mawe.201800066.

[2] W.J.S. Dolla, B.A. Fricke, B.R. Becker, Structural and drug diffusion models of conventional and auxetic drug-eluting stents, J. Med. Dev. Trans. ASME 1 (1) (Mar. 2007) 47–55, https://doi.org/10.1115/1.2355691.

[3] Y. Baradaran, M. Baghani, M. Kazempour, S.K. Hosseini, M. Karimpour, M. Baniassadi, Design and shape optimization of a biodegradable polymeric stent for curved arteries using FEM, Front. Mech. Eng. 7 (May 2021), https://doi.org/10.3389/fmech.2021.689002.

[4] C.R. Huang, W.D. Pan, H.Q. Chen, A.L. Copley, Thixotropic properties of whole blood from healthy human subjects, Biorheology 24 (6) (Dec. 1987) 795–801, https://doi.org/10.3233/BIR-1987-24630.

[5] M. Aenis, A.P. Stancampiano, A.K. Wakhloo, B.B. Lieber, Modeling of flow in a straight stented and nonstented side wall aneurysm model, J. Biomech. Eng. 119 (2) (May 1997) 206–212, https://doi.org/10.1115/1.2796081.

[6] L. Xingting, C. Xingyu, Z. Yunwu, X. Jie, J. Xingcan, D. Tingting, Z. Yongfeng, D. Toghraie, M. Zarringhalam, The thermal behavior of blood flow in the arteries with various radii and various stenosis angles using non-Newtonian Sisko model, Alex. Eng. J. 61 (9) (Sep. 2022) 7195–7201, https://doi.org/10.1016/j.aej.2021.12.063.

[7] M. Sohail, U. Nazir, Y.M. Chu, W.A. Kouz, P. Thounthong, Bioconvection phenomenon for the boundary layer flow of magnetohydrodynamic Carreau liquid over a heated disk, Sci. Iran. 28 (3 F) (Dec. 2021) 1896–1907, https://doi.org/10.24200/SCI.2021.53970.3518.

[8] L. Zhu, Q. Li, Y. Gao, L. Wang, Y. Fan, Multi-objective structural optimization and degradation model of magnesium alloy ureteral stent, Medicine in Novel Technology and Devices 22 (Jun. 2024) 100291, https://doi.org/10.1016/j.medntd.2024.100291.

[9] D. R. H. J. C. S. R. B. J. G. Andrew Cassar, Chronic coronary artery disease: diagnosis and management, in: Mayo Clinic Proceedings, vol. 84, 2009, pp. 1130–1146, 12.

[10] J. Canfield, H. Totary-Jain, 40 Years of percutaneous coronary intervention: history and future directions, J. Personalized Med. 8 (4) (Oct. 2018) 33, https://doi.org/10.3390/jpm8040033.

[11] S. Darba, N. Safaei, A.M. Ahari, S. Nosratnejad, G. Alizadeh, H. Ameri, M. Yousefi, Direct and indirect costs associated with coronary artery (heart) disease in tabriz, Iran, Risk Manag. Healthc. Pol. 13 (Jul. 2020) 969–978, https://doi.org/10.2147/RMHP.S261612.

[12] J. Iqbal, J. Gunn, P.W. Serruys, Coronary stents: historical development, current status and future directions, Br. Med. Bull. 106 (1) (Jun. 2013) 193–211, https://doi.org/10.1093/bmb/ldt009.

[13] J.A. Grogan, S.B. Leen, P.E. McHugh, Comparing coronary stent material performance on a common geometric platform through simulated bench testing, J. Mech. Behav. Biomed. Mater. 12 (Aug. 2012) 129–138, https://doi.org/10.1016/j.jmbbm.2012.02.013.

[14] W. Jiang, W. Zhao, T. Zhou, L. Wang, T. Qiu, A review on manufacturing and post-processing technology of vascular stents, Micromachines 13 (1) (Jan. 2022) 140, https://doi.org/10.3390/mi13010140.

[15] S.T. Alam, A.Q. Ansari, S. Urooj, M. Aldobali, A review based on biodegradable and bioabsorbable stents for coronary artery disease, Procedia Comput. Sci. 152 (2019) 354–359, https://doi.org/10.1016/j.procs.2019.05.006.

[16] F. Ahadi, M. Azadi, M. Biglari, M. Bodaghi, A. Khaleghian, Evaluation of coronary stents: a review of types, materials, processing techniques, design, and problems, Heliyon 9 (2) (Feb. 2023) e13575, https://doi.org/10.1016/j.heliyon.2023.e13575.

[17] F. Etave, G. Finet, M. Boivin, J.-C. Boyer, G. Rioufol, G. Thollet, Mechanical properties of coronary stents determined by using finite element analysis, J. Biomech. 34 (8) (Aug. 2001) 1065–1075, https://doi.org/10.1016/S0021-9290(01)00026-4.

[18] P.K.M. Prithipaul, M. Kokkolaras, D. Pasini, Assessment of structural and hemodynamic performance of vascular stents modelled as periodic lattices, Med. Eng. Phys. 57 (2018) 11–18, https://doi.org/10.1016/j.medengphy.2018.04.017.

[19] K. Kolandaivelu, R. Swaminathan, W.J. Gibson, V.B. Kolachalama, K.-L.N. Ehrenreich, V.L. Giddings, L. Coleman, G.K. Wong, E.R. Edelman, Stent thrombogenicity early in high-risk interventional settings is driven by stent design and deployment and protected by polymer-drug coatings, Circulation 123 (13) (Apr. 2011) 1400–1409, https://doi.org/10.1161/CIRCULATIONAHA.110.003210.

[20] N. Eshghi, M.H. Hojjati, M. Imani, A.M. Goudarzi, Finite element analysis of mechanical behaviors of coronary stent, Procedia Eng. 10 (2011) 3056–3061, https://doi.org/10.1016/j.proeng.2011.04.506.

[21] H. Hermawan, D. Dube, D. Mantovani, Developments in metallic biodegradable stents, Acta Biomater. 6 (5) (May 2010) 1693–1697, https://doi.org/10.1016/j.actbio.2009.10.006.

[22] W. Maamoun, Safety and efficacy of biodegradable polymer-coated biolimus-eluting stents, The Egyptian Heart Journal 65 (3) (2013) 207–212, https://doi.org/10.1016/j.ehj.2012.10.001.

[23] B. Obrien, W. Carroll, The evolution of cardiovascular stent materials and surfaces in response to clinical drivers: a review, Acta Biomater. 5 (4) (May 2009) 945–958, https://doi.org/10.1016/j.actbio.2008.11.012.

[24] D.M. Martin, F.J. Boyle, Drug-eluting stents for coronary artery disease: a review, Med. Eng. Phys. 33 (2) (Mar. 2011) 148–163, https://doi.org/10.1016/j.medengphy.2010.10.009.

[25] N. Li, H. Zhang, H. Ouyang, Shape optimization of coronary artery stent based on a parametric model, Finite Elem. Anal. Des. 45 (6–7) (May 2009) 468–475, https://doi.org/10.1016/j.finel.2009.01.001.

[26] A. Colombo, G. Stankovic, J.W. Moses, Selection of coronary stents, J. Am. Coll. Cardiol. 40 (6) (2002) 1021–1033, https://doi.org/10.1016/S0735-1097(02)02123-X.

[27] S. Garg, P.W. Serruys, Coronary stents, J. Am. Coll. Cardiol. 56 (10) (Aug. 2010) S43–S78, https://doi.org/10.1016/j.jacc.2010.06.008.

[28] C. Rogers, E.R. Edelman, Endovascular stent design dictates experimental restenosis and thrombosis, Circulation 91 (12) (Jun. 1995) 2995–3001, https://doi.org/10.1161/01.CIR.91.12.2995.

[29] V. Finazzi, F. Berti, L. Petrini, B. Previtali, A.G. Demir, Additive manufacturing and post-processing of superelastic NiTi micro struts as building blocks for cardiovascular stents, Addit. Manuf. 70 (May 2023) 103561, https://doi.org/10.1016/j.addma.2023.103561.

[30] V. Chausse, E. Casanova-Batlle, C. Canal, M.-P. Ginebra, J. Ciurana, M. Pegueroles, Solvent-cast direct-writing and electrospinning as a dual fabrication strategy for drug-eluting polymeric bioresorbable stents, Addit. Manuf. 71 (Jun. 2023) 103568, https://doi.org/10.1016/j.addma.2023.103568.

[31] J.M. Garasic, E.R. Edelman, J.C. Squire, P. Seifert, M.S. Williams, C. Rogers, Stent and artery geometry determine intimal thickening independent of arterial injury, Circulation 101 (7) (Feb. 2000) 812–818, https://doi.org/10.1161/01.CIR.101.7.812.

[32] J.J. Wentzel, R. Krams, J.C. Schuurbiers, J.A. Oomen, J. Kloet, W.J.v.D. Giessen, P.W. Serruys, C.J. Slager, Relationship between neointimal thickness and shear stress after wallstent implantation in human coronary arteries, Circulation 103 (13) (Apr. 2001) 1740–1745, https://doi.org/10.1161/01.CIR.103.13.1740.

[33] J.F.L. Jr, L.E. Olson, R.C. Molthen, D.A. Hettrick, P.F. Pratt, M.D. Hardel, J.R. Kersten, D.C. Warltier, P.S. Pagel, Alterations in wall shear stress predict sites of neointimal hyperplasia after stent implantation in rabbit iliac arteries, Am. J. Physiol. Heart Circ. Physiol. 288 (5) (2004) H2465–H2475, https://doi.org/10.1152/ajpheart.01107. May 2005.

[34] F. Gijsen, Y. Katagiri, P. Barlis, C. Bourantas, C. Collet, U. Coskun, J. Daemen, J. Dijkstra, E. Edelman, P. Evans, K.v.d. Heiden, R. Hose, B.-K. Koo, R. Krams, A. Marsden, F. Migliavacca, Y. Onuma, A. Ooi, E. Poon, H. Samady, P. Stone, K. Takahashi, D. Tang, V. Thondapu, E. Tenekecioglu, L. Timmins, R. Torii,

J. Wentzel, P. Serruys, Expert recommendations on the assessment of wall shear stress in human coronary arteries: existing methodologies, technical considerations, and clinical applications, Eur. Heart J. 40 (41) (Nov. 2019) 3421–3433, https://doi.org/10.1093/eurheartj/ehz551.
[35] S. Beier, J. Ormiston, M. Webster, J. Cater, S. Norris, P. Medrano-Gracia, A. Young, B. Cowan, Hemodynamics in idealized stented coronary arteries: important stent design considerations, Ann. Biomed. Eng. 44 (2) (Feb. 2016) 315–329, https://doi.org/10.1007/s10439-015-1387-3.
[36] R. Gharleghi, H. Wright, V. Luvio, N. Jepson, Z. Luo, A. Senthurnathan, B. Babaei, B.G. Prusty, T. Ray, S. Beier, A multi-objective optimization of stent geometries, J. Biomech. 125 (Aug. 2021) 110575, https://doi.org/10.1016/j.jbiomech.2021.110575.
[37] G.P. Annanto, R. Ismail, I. Haryanto, M. Ariyanto, K.A. Pambudi, K.A. Pranoto, Numerical analysis of stress and displacement on the index finger of the prosthetic hand due to hook position. Exploring Resources, Process and Design for Sustainable Urban Development: Proceedings of the 5th International Conference on Engineering, Technology, and Industrial Application, 2019 050017, https://doi.org/10.1063/1.5112461.
[38] J.M. Reverte, M.A. Caminero, J.M. Chacon, E. Garcia-Plaza, P.J. Nunez, J.P. Becar, Mechanical and geometric performance of PLA-based polymer composites processed by the fused filament fabrication additive manufacturing technique, Materials 13 (8) (Apr. 2020) 1924, https://doi.org/10.3390/ma13081924.
[39] G.M. Baer, T.S. Wilson, W. Small, J. Hartman, W.J. Benett, D.L. Matthews, D.J. Maitland, Thermomechanical properties, collapse pressure, and expansion of shape memory polymer neurovascular stent prototypes, J. Biomed. Mater. Res. B Appl. Biomater. 90B (1) (Jul. 2009) 421–429, https://doi.org/10.1002/jbm.b.31301.
[40] H.L. Simonetti, F. de Assis das Neves, V.S. Almeida, Multiobjective topology optimization with stress and strain energy criteria using the SESO method and a Multicriteria Tournament Decision, Structures 30 (Apr. 2021) 188–197, https://doi.org/10.1016/j.istruc.2021.01.002.
[41] X. Yan, Y. Xiong, D.W. Bao, Y.M. Xie, X. Peng, A Multi-volume constraint approach to diverse form designs from topology optimization, Eng. Struct. 279 (Mar. 2023) 115525, https://doi.org/10.1016/j.engstruct.2022.115525.
[42] M. Ebeling-Rump, D. Homberg, R. Lasarzik, Two-scale topology optimization with heterogeneous mesostructures based on a local volume constraint, Comput. Math. Appl. 126 (Nov. 2022) 100–114, https://doi.org/10.1016/j.camwa.2022.09.004.
[43] N.K. Putra, P.S. Palar, H. Anzai, K. Shimoyama, M. Ohta, Multiobjective design optimization of stent geometry with wall deformation for triangular and rectangular struts, Med. Biol. Eng. Comput. 57 (2019) 15–26.
[44] H. Li, J. Gu, M. Wang, D. Zhao, Z. Li, A. Qiao, B. Zhu, Multi-objective optimization of coronary stent using Kriging surrogate model, Biomed. Eng. Online 15 (2) (2016) 148.
[45] J.F. LaDisa, L.E. Olson, D.A. Hettrick, D.C. Warltier, J.R. Kersten, P.S. Pagel, Axial stent strut angle influences wall shear stress after stent implantation: analysis using 3D computational fluid dynamics models of stent foreshortening, Biomed. Eng. Online 4 (1) (Dec. 2005) 59, https://doi.org/10.1186/1475-925X-4-59.
[46] F. Ahadi, M. Biglari, M. Azadi, M. Bodaghi, Computational fluid dynamics of coronary arteries with implanted stents: effects of Newtonian and non-Newtonian blood flows, Engineering Reports (Sep. 2023), https://doi.org/10.1002/eng2.12779.
[47] B.K. Muniandy, Non-Newtonian computational fluid dynamics (CFD) modeling on blood clot extraction. Faculty of Chemical Engineering, University Technology PETRONAS, 2013.
[48] M.E.S. Elamin, A.M. A Seory, Study of an Artificial Heart: Design and Simulation, Faculty of Engineering, University of Khartoum, 2016.
[49] M.S. Elliott, J.S. Cole, R.W. Blair, G.H. Menary, Highlighting hemodynamic risks for bioresorbable stents in coronary arteries, Fluids 8 (9) (Aug. 2023) 241, https://doi.org/10.3390/fluids8090241.
[50] J.F. LaDisa, L.E. Olson, H.A. Douglas, D.C. Warltier, J.R. Kersten, P.S. Pagel, Alterations in regional vascular geometry produced by theoretical stent implantation influence distributions of wall shear stress: analysis of a curved coronary artery using 3D computational fluid dynamics modeling, Biomed. Eng. Online 5 (1) (Dec. 2006) 40, https://doi.org/10.1186/1475-925X-5-40.
[51] R. van Lith, E. Baker, H. Ware, J. Yang, A.C. Farsheed, C. Sun, G. Ameer, 3D-Printing strong high-resolution antioxidant bioresorbable vascular stents, Advanced Materials Technologies 1 (9) (Dec. 2016), https://doi.org/10.1002/admt.201600138.